

UNITED STATES DEPARTMENT OF COMMERCE

WEATHER BUREAU



U.S. NATIONAL METEOROLOGICAL CENTER, Suitland, Md.
TECHNICAL MEMORANDUM NO. 26

EXPERIMENTS IN 1000 MB PROGNOSIS

by

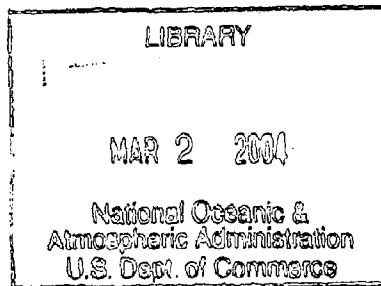
Richard J. Reed
National Meteorological Center

RAREBOOK

QC
996

.T33

no. 26



Washington, D. C.

1963

124 788

National Oceanic and Atmospheric Administration

U.S. Joint Numerical Weather Prediction Unit

ERRATA NOTICE

One or more conditions of the original document may affect the quality of the image, such as:

Discolored pages

Faded or light ink

Binding intrudes into the text

This has been a co-operative project between the NOAA Central Library, National Center for Environmental Prediction and the U.S. Air Force. This project includes the imaging of the full text of each document. To view the original documents, please contact the NOAA Central Library in Silver Spring, MD at (301) 713-2607 x124 or www.reference@nodc.noaa.gov.

LASON

Imaging Contractor

12200 Kiln Court

Beltsville, MD 20704-1387

April 13, 2004

1. INTRODUCTION

Despite the success achieved by the barotropic model in numerically predicting the flow pattern at 500 mb, corresponding progress has not been made in attaining useful 1000 mb surface prognoses by simple two-level baroclinic models. The present* operational model (mesh model), which is obtained by extrapolating the forecast 850-500 mb thickness from the 850 mb level to the 1000 mb level, suffers, in the eyes of the subjective forecasters, from an inability to predict cyclogenesis and from a general oversmoothness and diffuseness of pattern. Small scale features tend to disappear during the forecast interval and sharp features, such as frontal troughs, tend to lose their identities.

As a consequence of these and other deficiencies of the present numerical 1000 mb prognoses, the standard method employed by the forecasters at the Analysis and Forecast Branch of the National Meteorological Center in preparing surface prognostic charts involves the fitting of a consistent isobaric pattern to the 500 mb vorticity pattern (obtained from the barotropic forecast) in accordance with well established empirical rules. Frequently, corrections are made to the barotropic prognoses on the basis of experience with typical errors, and these corrections are incorporated in the surface prognoses as well.

Because of the comparative ease with which the forecaster is able to fit surface features to the upper-level vorticity pattern, it might be hoped that even a simple two-level forecast model would be capable of yielding a useful 1000 mb

* May 1962

counterpart to the barotropic forecast. However, as we have just noted, this hope is not supported by numerical experiments conducted in the past in the Development Branch at the National Meteorological Center. However, other experiments carried out over an extended period of time by the writer and by Professor Sanders of M. I. T., based on graphical solutions of a two-level model, have appeared to give useful results. As an example of apparently useful graphical prognoses, we may cite the series presented by Reed (1960), which were found to be comparable in accuracy to the corresponding subjective prognoses issued by the Analysis and Forecast Branch. In the discussion of the typical errors in this series, it was noted that the most serious probably stemmed from the fact that only initial, rather than initial and forecast, 500 mb patterns were available. Thus even better results were to be anticipated if barotropic forecasts were utilized in the procedure.

More recently a short series of graphical prognoses were prepared at the Analysis and Forecast Branch under Professor Sander's supervision by forecasters without previous experience with the method. These, also, achieved the same level of accuracy as the subjective prognoses, though in this later experiment prognostic 500 mb charts were used.

Encouraged by the results of these later tests, the directors of the Analysis and Forecast Branch requested the writer to program the model for the IBM 7090 so that current forecasts could be obtained on a twice daily basis and evaluated for their usefulness by experienced forecasters. It must be stated frankly that on logical grounds there was little, if any, reason to feel that the numerical solutions of the

equations used in graphical prediction should differ in any significant way from earlier solutions which were tried and found wanting. The present model and all earlier models have involved only two levels of information and essentially the same modelling assumptions.

However, one difference which could conceivably lead to improvement, by reducing the truncation error, is the use of a relatively slow-varying equivalent advecting wind in the graphical method. Another difference which might have some effect arises from the different order of solution of the basic equations. The vertical motion is first eliminated, and the 1000 mb height is then forecast directly by use of the barotropic 500 mb height prediction. A point of obvious, and perhaps important, difference with the mesh model is the use of 1000 mb rather than 850 mb as the lowest level of information. However, the predecessor to the mesh model, the so-called thermotropic model, did utilize 1000 mb data.

A final peculiarity of the graphical prediction method, which, if carried into the numerical solution of the equations, might produce noticeably different results, is the use of Lagrangian rather than Eulerian integrations. However, many of the library routines available in the computing branch are better adapted to the fixed grid point than to the moving particle type of computation, and for this reason the first forecast experiment was carried out by hourly iterations at the fixed grid points. More than five months of twice daily 1000 mb prognoses have now been obtained in this first experiment, and definite impressions have been gained concerning the usefulness and shortcomings of the solutions. Sample forecasts will

be presented in section 3.

In the course of this first experiment the suspicion arose that the equations were not being accurately solved by the Eulerian method, presumably because of truncation error. It seemed that in certain cases the conserved quantity (essentially the potential vorticity) which appears in the equations was not being conserved in the advections and iterations. Moreover occasional ragged and exaggerated patterns developed in the 24 to 36 hour forecasts which it was felt might be eliminated by a superior integration technique. The decision was therefore made to write a second program which utilized the same equations but which solved them by the Lagrangian technique of following individual air parcels. Strictly speaking, the solutions are only quasi-Lagrangian, combining trajectory tracing and computations at fixed grid points in the manner discussed by Okland (1962).

The main purpose of the present memorandum is to describe and compare the results of the two experiments in 1000 mb prognosis. In section 2, the modelling assumptions and computational procedures of the Eulerian experiment are reviewed. The results of the experiment are evaluated subjectively in section 3 and some sample forecasts are shown. The background of the quasi-Lagrangian experiment is outlined in section 4. Finally comparisons of the Eulerian and Lagrangian solutions in a limited number of cases are presented in section 5.

2. THEORETICAL BACKGROUND AND COMPUTATIONAL PROCEDURES FOR EXPERIMENT 1

Derivations of the graphical prediction equations have been given previously by Estoque (1957) and Reed (1957). In practice a short, approximate method of

solution first suggested by Estoque has been found satisfactory. In this method the space-mean 1000 mb wind field is neglected compared with the wind field itself, making relaxation unnecessary and thereby considerably shortening the hand procedures. It was decided to conduct the first numerical experiment also without relaxation. However, a different approach has been followed here in deriving the equations in order to eliminate a logical difficulty which arises in Estoque's treatment. When the space mean 1000 mb wind is neglected, the mesh length is not defined, yet this quantity still appears as a major parameter of the model.

The vorticity equation may be written

$$\frac{\partial}{\partial t} (\zeta_0 + f) = -V_0 \cdot \nabla (\zeta_0 + f) + f \left(\frac{\partial \omega}{\partial p} \right)_0 \quad (1)$$

where ζ is the vorticity, f the coriolis parameter, V the horizontal wind velocity and ω the vertical motion (dp/dt). The subscript zero indicates the 1000 mb level.

We next assume a parabolic vertical velocity profile between the surface and 500 mb (subscript 5).

$$\omega = \omega_0 + (\omega_5 - \omega_0) \left[1 - \left(\frac{p - p_5}{p_0 - p_5} \right)^2 \right] \quad (2)$$

which when substituted in (1) yields

$$\frac{\partial}{\partial t} (\zeta_0 + f) = -V_0 \cdot \nabla (\zeta_0 + f) - \frac{2f}{p_0 - p_5} (\omega_5 - \omega_0) \quad (3)$$

If now the geostrophic wind is used to approximate the vorticity and if, furthermore, the surface pressure pattern is, to a first approximation, regarded as consisting of equally spaced, circular highs and lows in a uniform basic current

so that

$$Z_0 = A(y) + B \sin \frac{2\pi}{L} x \sin \frac{2\pi}{L} y \quad (4)$$

it follows that

$$\int_0 = \frac{g}{f} \nabla^2 Z_0 = - \frac{8\pi^2 g}{f L^2} Z_0 \quad (5)$$

Here g is the acceleration of gravity, L is the wave length, and Z_0 the 1000 mb height.

Substitution of (5) in (3) yields the equation

$$\frac{\partial}{\partial t} (-Z_0 + G') = -V_0 \cdot \nabla (-Z_0 + G') - \frac{f^2 L^2}{4\pi g} \frac{\omega_5 - \omega_0}{p_0 - p_5} \quad (6)$$

where

$$G' = \frac{f^2 L^2}{16\pi^2 g}$$

Equation (6) involves the approximation that the variation of $1/f$ may be neglected in comparison with the variation of Z_0 .

The thermodynamic energy equation

$$\frac{\partial}{\partial t} \left(\frac{\partial Z}{\partial p} \right) = -V \cdot \nabla \frac{\partial Z}{\partial p} - \sigma \omega \quad (7)$$

where

$$\sigma = - \frac{\alpha}{g\theta} \frac{\partial \theta}{\partial p}$$

is next introduced. The symbols α and θ denote the specific volume and potential temperature, respectively.

With the assumption of a straight line hodograph in the layer between 1000 mb and 500 mb, equation (7) may be integrated to give

$$\frac{\partial}{\partial t} (Z_5 - Z_0) = -V_0 \cdot \nabla (Z_5 - Z_0) + \frac{\sigma (p_0 - p_5)}{3} (2\omega_5 + \omega_0) \quad (8)$$

Next we multiply (8) by

$$k' = \frac{3}{8\pi^2} \frac{f^2 L^2}{g \sigma (p_0 - p_s)^2} \quad (8a)$$

a slow varying parameter which will be regarded as constant, and add to (6) giving

$$\frac{\partial}{\partial t} [-Z_0 + G' + k'(Z_s - Z_0)] = -W_0 \cdot \nabla [-Z_0 + G' + k'(Z_s - Z_0)] + \frac{3}{8\pi^2} \frac{f^2 L^2}{g (p_0 - p_s)} \omega_0 \quad (9)$$

Introducing now the kinematic boundary condition

$$\omega_0 = W_{g_0} \cdot \nabla p_G$$

where p_G is the pressure at the ground, we find that

$$\frac{\partial}{\partial t} [-Z_0 + G' - M' + k'(Z_s - Z_0)] = -W_0 \cdot \nabla [-Z_0 + G' - M' + k'(Z_s - Z_0)] \quad (10)$$

where

$$M' = \frac{3}{8\pi^2} \frac{f^2 L^2}{g} \frac{p_G}{p_0 - p_s}$$

Equation (10) is now rearranged to give

$$\frac{\partial}{\partial t} [k' Z_s - (1+k') Z_0 + G' - M'] = -W_0 \cdot \nabla [k' Z_s - (1+k') Z_0 + G' - M'] \quad (11)$$

or

$$\frac{\partial}{\partial t} [k Z_s - Z_0 + G - M] = -W_0 \cdot \nabla [k Z_s - Z_0 + G - M] \quad (12)$$

where

$$k = k' / (1+k') \quad (12a)$$

$$G = G' / (1+k')$$

$$M = M' / (1+k')$$

We next make use of the idea, first introduced by Fjortoft (1952), of an equivalent advecting wind, which gives the same instantaneous advection as \mathbb{V}_0 but which has the property of changing more slowly with time. This concept is particularly valuable in graphical integration where long time steps must be employed.

Thus (12) may be written in the equivalent form

$$\frac{\partial}{\partial t} (k Z_5 - Z_0 + G - M) = -\mathbb{V}_E \cdot \nabla (k Z_5 - Z_0 + G - M) \quad (13)$$

where

$$\mathbb{V}_E = 1K \times \frac{g}{f} \nabla (k Z_5 + G - M)$$

and

$$\mathbb{V}_0 = 1K \times \frac{g}{f} \nabla Z_0$$

The form of the prediction equation in (13) is especially useful in graphical solutions where it is desired to trace the movement of a conservative quantity.

For numerical solution, it is convenient to write (13) in the alternative form

$$\frac{\partial Z_0}{\partial t} = -\mathbb{V}_E \cdot \nabla Z_0 + k \frac{\partial Z_5}{\partial t} \quad (14)$$

For the avoidance of an artificial long-scale build-up of the conservative quantity, it is desirable that the field of \mathbb{V}_E should be nondivergent (Shuman 1957).

Thus \mathbb{V}_E has been expressed in the following form

$$\mathbb{V}_E = 1K \times \frac{g}{f_{45}} \nabla (k \psi_5 + G - M)$$

where Ψ_5 is the 500 mb stream function, in height units, determined from the balance equation. With this relationship (14) becomes

$$\frac{\partial Z_0}{\partial t} = \frac{f}{f_{45}} \left[\left(\frac{\partial Z_E}{\partial y} \frac{\partial Z_0}{\partial x} - \frac{\partial Z_E}{\partial x} \frac{\partial Z_0}{\partial y} \right) + k \frac{\partial \Psi_5}{\partial t} \right] \quad (15)$$

where $Z_E = k \Psi_5 + G - M$

The forecast procedure is to solve (15) by means of finite difference approximations for the 1000 mb height tendency. At the initial hour the one-hour change is added to the initial value. In subsequent iterations the change is computed for two hours and is added to the height value for the previous hour to obtain the value for the later hour. The 1000 mb heights and 500 mb stream functions required for the solution of (15) are taken from the analysis and barotropic history tapes.

The value of k used in the computations is 0.55. This value was empirically determined from experience with graphical predictions, and, for a standard static stability and latitude of 45° , corresponds to a predominant wave number, as defined by (8a) and (12a), of six. The corresponding value of M is found to be $.088 p_G$.

Early testing revealed that the influence of the G -term was negligible. It was also found that a smaller value of the coefficient of p_G gave better results, and the value was arbitrarily reduced to .066. Furthermore, over level ground it appeared that the advection of Z_0 was somewhat larger than given by use of the

coefficient of 0.55 with ψ_5 . It was therefore decided to raise this coefficient by the factor 1.13. This same factor is used in correcting the truncation error in the advection term of the barotropic forecasts. The quantity Z_E used in practice was thus

$$Z_E = 0.62 \psi_5 - 0.066 p_G \quad (16)$$

In measuring the advection term in equation (15) a 16-point Jacobian devised by Shuman was used. Every twelve hours the predicted field was smoothed by means of the regular operational smoother.

3. RESULTS OF EXPERIMENT 1

An objective verification system has not been employed in evaluating the results of the experiment. Instead the performance of the forecasts has been judged on the basis of subjective impressions of forecasters in the Analysis and Forecast Branch acquired through their daily experiences with the 12, 24, and 36 hour 1000 mb prognoses and the 36 hour thickness prognosis.

The general, overall impression is that the objective prognoses represent useful caricatures of the verification chart, though in individual cases quite accurate and realistic patterns may be forecast (figures 1 and 2). There seems to be no doubt that the important features of the pressure pattern - the pressure centers, trough and ridge lines - represent, day in and day out, a good fit to the corresponding barotropic forecast so that when the upper-level forecast is accurate, the 1000 mb prognosis is broadly correct. But even when grossly correct, the

prognoses tend to have exaggerated and sometimes ragged features which detract from their usefulness. An example of a particularly distorted prognosis appears in figure 3. High pressure systems tend almost invariably to overbuild. The lows show a corresponding, but not so pronounced, tendency to deepen. Once a low has achieved its maximum depth, it generally weakens at a much lesser rate than observed.

The tendency for the development of exaggerated and distorted features has been observed to some degree in graphical solutions. However, perhaps because of the forecaster's habit of introducing subjective smoothing, the development has not been nearly so marked. On the other hand, in several extreme cases of excessive intensification in the numerical forecasts, it appeared from cursory examination that the conservative quantity was not in fact being conserved. It was this observation that led to the establishment of the second, Lagrangian experiment. Not only was it hoped that a different method of solution would lead to improved results, but it was considered desirable, as a matter of basic interest, to conduct an experiment in which the two mathematically equivalent methods of solution could be compared.

Other characteristic failings of the model, noted in previous graphical tests, appeared again in the current series. Cold highs which moved offshore in winter were forecast to be much stronger than observed. Even the crude introduction of diabatic heating into the model would no doubt partly eliminate this error (Reed, 1958). Another characteristic error appeared just east of the Rocky Mountains when

shallow cold air was wedged against the east slopes. In such cases inverted troughs in Mexico or the Southern Rockies were forecast to move eastward too rapidly, or the southward push of a cold ridge of high pressure along the east slope was not correctly gauged. It was formerly thought that the apparently abnormal southward surge of high pressure is connected with an extreme southward directed ageostrophic component in cold air which resists being forced up the east slope of the mountains. However, it seems from some closer examinations that the appearance of ageostrophic motion, in excess of the usual frictional outflow, may be an illusion connected with the fictitious nature of the pressure gradients on the surface chart. When winds and isobars (or pressure contours) are compared at the same level, and not along the sloping surface defined by the terrain, the angle between them is not noticeably larger than the frictional angle over level ground. Figures 4 and 5 furnish an example of a case in which large forecast errors propagated downstream (in terms of the 500 mb flow) from the lee slopes of the Rockies. Clearly the NW-SE inclination of the reduced isobars in western Texas agrees neither with the 850 mb flow nor the surface wind flow (making due allowance for friction).

The general impression is that the orographic and diabatic errors are of great importance in the winter forecasts. Until they are eliminated, numerical methods will be powerless to handle such critical problems as secondary cyclogenesis along the east coast of the United States. Sangster (1960) has presented a method for obtaining an accurate representation of the pressure gradient force in mountainous

terrain. From his work it is apparent that more complex models which allow for variation in static stability are needed before the orographic effect can be adequately handled, and the same is probably true for the heating effects.

4. THEORETICAL BACKGROUND AND COMPUTATIONAL PROCEDURES FOR EXPERIMENT 2

The derivation of the equations proceeds as in section 2 except that now

$$f_0 = \frac{g}{f} \nabla^2 Z_0 = \frac{4g m^2}{f d^2} (\bar{Z}_0 - Z_0) \quad (17)$$

where d is the mesh length, m the map scale factor and the bar indicates the average of Z_0 at the four grid points surrounding the point of interest. Thus equation (16) is replaced by the following equation

$$\frac{\partial}{\partial t} (\bar{Z}_0 - Z_0 + G) = -V_0 \cdot \nabla (\bar{Z}_0 - Z_0 + G) - \frac{f^2 d^2}{2g m^2} \left(\frac{\omega_5 - \omega_0}{p_0 - p_5} \right) \quad (18)$$

The thermodynamic energy equation (8) remains exactly as before. This is now multiplied by

$$b' = \frac{3}{4} \frac{f^2 d^2}{g m^2 \sigma} \frac{1}{(p_0 - p_5)^2} \quad (18a)$$

and added to (18) to give

$$\frac{\partial}{\partial t} [\bar{Z}_0 - Z_0 + G' + b'(Z_5 - Z_0)] = -V_0 \cdot \nabla [\bar{Z}_0 - Z_0 + G' + b'(Z_5 - Z_0)] + \frac{3 f^2 d^2 \omega_0}{4 g m^2 (p_0 - p_5)} \quad (19)$$

which upon introduction of the boundary condition assumes the form of a conservation law

$$\frac{\partial}{\partial t} [\bar{Z}_0 - Z_0 + G' + b'(Z_5 - Z_0) - M'] = -V_0 \cdot \nabla [\bar{Z}_0 - Z_0 + G' + b'(Z_5 - Z_0) - M'] \quad (20)$$

where

$$M' = \frac{3 f^2 d^2}{4 g m^2} \frac{\rho_a}{\rho_0 - \rho_s}$$

Upon rearrangement (20) may be written

$$\frac{\partial}{\partial t} [a \bar{z}_0 - z_0 + b z_s + a G' - a M'] = -V_0 \cdot \nabla [a \bar{z}_0 - z_0 + b z_s + a G' - M'] \quad (21)$$

Here

$$\begin{aligned} a &= 1/(1+b') \\ b &= b'/(1+b') \end{aligned} \quad (21a)$$

Again the concept of an equivalent advecting wind is introduced. Thus

$$V_E = K \times \frac{g}{f} \nabla (a \bar{z}_0 + b z_s + G - M) \quad (22)$$

which may be adequately approximated by

$$V_E = K \times \frac{g}{f_{45}} \nabla (b z_s - M) \quad (23)$$

With this wind, and the definitions $G = aG'$, $M = aM'$, (21) becomes

$$\frac{\partial}{\partial t} (a \bar{z}_0 - z_0 + b z_s + G - M) = -V_E \cdot \nabla (a \bar{z}_0 - z_0 + b z_s + G - M) \quad (24)$$

This equation states that the quantity in parentheses is conserved in the equivalent wind field. Thus

$$(a \bar{z}_0 - z_0 + b z_s + G - M)_p = (a \bar{z}_0 - z_0 + b z_s + G - M)_u \quad (25)$$

where the subscripts p and u refer to predicted-downstream and initial-upstream quantities, respectively.

In the quasi-Lagrangian scheme equation (25) is used to make 12-hourly predictions of the 1000 mb height at the 1977 grid points of the standard JNWP grid.

Twelve-hour trajectories are traced back upstream from the grid points, and the various upstream quantities on the right hand side of (25) are found by means of quadratic interpolation from the known initial values at the grid points. The predicted 500 mb height is known from the barotropic forecast. The predicted values of G and M are known for all time for each grid point. Thus (25) becomes a Helmholtz equation of the form

$$a \bar{Z}_{op} - Z_{op} + A = 0 \quad (26)$$

which is solvable for Z_{op} by the relaxation method. The quantity A is defined as

$$A = \left[(b Z_5 + G - M)_p + (Z_0 - b Z_5 - G + M)_u \right] - a \bar{Z}_{ou}$$

A short method of solving for Z_{op} , analogous to the previous solution, results when variations of $(a \bar{Z}_0)$ are neglected compared with variations of Z_0 . Then

$$Z_{op} = (Z_0 - b Z_5 - G + M)_u + (b Z_5 + G - M)_p \quad (27)$$

This solution was used in making the comparisons between the Lagrangian and Eulerian methods. It also serves as a first guess for the relaxation method. It will be recalled that relaxation was added in the second program in the hope of removing the raggedness and distortions from future forecasts.

Some of the more important details of the computations will now be discussed. The trajectories were constructed in hourly steps using winds at time t to determine the displacements during the interval from t to t - 1. As shown in the appendix, the failure to take account of time and space variations of the advecting wind field does

not lead to significant error for the short time interval employed. Displacements were first computed at the fixed-grid points from differences of $b\psi - M$ taken over a double grid interval. A bi-linear interpolation was used in determining the displacement of the moving air particle which in general lay between the fixed grid points. The interpolation formula is given in the appendix.

Once the position of each coordinate is known at the beginning of the 12-hour forecast period, the next step is to determine the quantity on the right hand side of (25). This is accomplished by the bi-quadratic interpolation formula given in the appendix. In computing the initial fixed grid values of $(a \bar{Z}_0)$, a 16 point averaging formula was used. It was felt that a more representative average would be obtained by including a greater number of points. The formula is explained more fully in the appendix.

The grid interval over which the averaging was performed was twice the standard grid interval of 381 km. The choice of grid interval was determined empirically in the manner of the wave length or wave number in Experiment 1. The coefficient b which corresponds to k in the previous solution was assigned the value 0.55. Equations (18a) and (21a) were then solved for the mesh length which turned out to be 775 km or approximately twice the regular length.

Once the effective grid distance is known, the numerical "constants" in G and M are determined. Thus these quantities are found to be

$$G = 1.63 \times 10^4 \sin^2 \phi \quad (\text{cgs})$$
$$M = 0.0405 \rho_G \quad (\text{cgs})$$

Because of the 16-point averaging formula, the relaxation can be carried out only within the inner area bounded by the dashed lines in figure 6. At exterior points Z_0 was held constant at

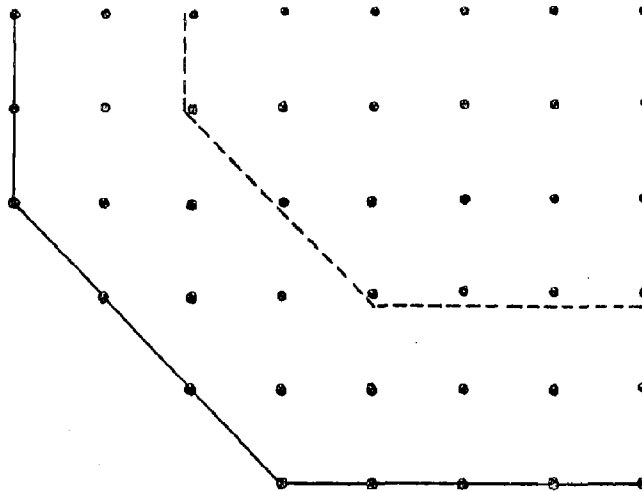


Figure 6

Illustration of boundary (dashed line) separating interior and exterior regions

the initial value. The dashed line was also regarded as the exterior boundary in measuring trajectories, since it was not possible to apply the bi-quadratic interpolation formula in most of the outer strip. When air particles crossed the dashed boundary, their grid indices were rounded off to whole numbers causing the floating points to be displaced to fixed grid points. Thus air which entered the interior during the forecast interval was assumed to originate at grid points on, or one grid distance removed from, the interior boundary. Since the exterior points are located well within the tropics, the assignment of incorrect origins to certain trajectories is not believed to have a significant effect on the forecasts.

5. RESULTS OF EXPERIMENT 2

The original intent in this second experiment was to rerun about a dozen forecasts in which the Eulerian solution exhibited large errors of certain characteristic types and to compare the two solutions. Because of availability of data tapes, the test cases had to be chosen for the period following March 5, 1962, though better examples of errors occurred in earlier cases. Moreover, once the cases were selected, various difficulties were experienced in retrieving the data, and certain cases had to be abandoned. The tests therefore are limited to five cases which exhibited characteristic errors in the Eulerian solution and to a single case (see figure 1) in which the Eulerian solution was highly accurate. If only cases of extreme error are chosen the odds would seem to favor improvement for any reasonable alternative solution. Thus, it was felt necessary to determine whether the Lagrangian scheme could improve bad forecasts without damaging good.

Experience with the Eulerian forecasts led to recognition of four severe types of forecast deficiencies. These we have labelled (1) exploding highs (2) teardrop highs, (3) southeast extensions and (4) distorted, unrealistic shapes. The exploding high is characterized by excessively high central pressure and strong gradients near the high center, as in an intense low. The teardrop high consists of an abnormal ridge development, generally beneath the jet stream in the south and southwest quadrants of occluded cyclones, which takes the form of a teardrop. The southeast extension refers to the occasional tendency for an elongated trough of low pressure to develop in the southeast quadrants of lows. Each of these features gives an unrealistic appearance to the forecast. However, other less distinctive types of distortion occur which in extreme cases we refer to as distorted, unrealistic shapes.

It is not feasible to reproduce here the forecasts for each of the test cases. Instead a brief description and evaluation of each case will be given with only one case being selected for illustration. This is the case which contained the most severe errors and which showed the greatest difference between the two solutions. The Eulerian forecast for the situation in question has already been shown in figure 3.

Case of 00Z April 16, 1962 - Extreme development of exploding high over Rocky Mountains. Marked improvement noted in Lagrangian solution with central pressure reduced by 300 ft. in 36-hr. forecast.

Case of 12Z April 13, 1962 - Teardrop high and southeast extension south and southeast of Newfoundland. Also, development of "induced low" beneath the teardrop high, as sometimes noted in such cases. The Lagrangian solution removed the undesirable features and gave a much improved verification. (Compare figures 3, 7, and 8, the Eulerian and Lagrangian forecasts and verification, respectively.) The behavior of the conservative quantity (approximated by $\frac{1}{2} Z_s - Z_o$) during the development of the undesirable features of the Eulerian forecast is shown in figures 9 - 12. According to subjective estimates from trajectory tracing, the computational difficulties commence in the interval from 12 to 24 hours and are first manifested in the appearance of fictitious maxima and minima of the conservative quantity along the stream field. (Note the undulations of the 88 contour on the left side of figure 11. Twelve-hours later (figure 12) further amplification is evident; and a fictitious 92 high center has appeared east of Cape Hatteras.

Case of 12Z March 28, 1962 - Southeast extension from low near Lake Huron. In this case the feature was only moderately developed, and the Lagrangian solution failed to diminish it significantly.

Case of 00Z April 12, 1962 - Distorted, unrealistic shapes to pressure systems.

The Lagrangian forecast proved noticeably superior.

Case of 00Z March 21, 1962 - Probably the most successful Eulerian forecast during the five months of testing. The Lagrangian forecast was essentially the same and of equal quality.

In addition to the results of the above cases, forecasts were obtained for the randomly selected case used in checking out the Lagrangian program. Although the Eulerian solution in this case was lacking the extreme exaggerations of the test cases, it nevertheless contained minor distortions which were largely eliminated in the Lagrangian solution. The only forecast involving relaxation was also carried out on this case. The relaxation eliminated the slight remaining distortions and produced eye-pleasing patterns which represented an excellent fit to the corresponding barotropic 500 mb prognosis.

Because of the limited number of cases tested to date, it is perhaps a bit early to draw firm conclusions concerning the relative merits of the Eulerian and Lagrangian forecasts. But certainly the preliminary results lend strong support to the following tentative conclusions.

- (1) The Lagrangian solutions eliminate in whole or in part the four characteristic types of errors noted in the Eulerian forecasts.
- (2) The Lagrangian solutions give less ragged and more realistic looking pressure patterns.
- (3) Large scale overbuilding of highs and, to a lesser extent, overdeepening of lows is characteristic of both type of forecasts and appears to be a weakness of the two-level model.

From the theoretical standpoint perhaps the most interesting result of the experiment has been the demonstration of the growth, in specific instances, of large computational errors in the Eulerian forecasts. Since the use of a one hour time

step assures computational stability for the grid distances (roughly 300 km) and displacement speeds (60 knots) entering into the forecasts, these errors must be due to truncation effects. Such effects have been discussed by Obukhov (1957), Gates (1959), Phillips (1960), and Knox (1961) for the linear case of the advection of a conservative field by a uniform constant advecting wind. In the examples cited here the advected quantity is conserved, but the advecting wind changes both in time and space. Whether this is an additional factor in the pronounced growth of the parasitic waves encountered in the present experiments is a matter of conjecture. Further work on computational errors in nonlinear systems (Phillips, 1959) should shed light on this important question.

6. SUMMARY AND CONCLUSIONS

A two-level model used in making graphical predictions of 1000 mb height has been solved numerically both by normal finite-difference, iterative procedures and by a quasi-Lagrangian method involving 12 hour trajectories. Both methods employ the output of the 500 mb barotropic forecasts. Neither method involves relaxation, though the Lagrangian method has also been programmed to operate with relaxation in future tests.

Twelve, twenty-four and thirty-six hour 1000 mb prognoses and thirty-six hour 1000-500 mb thickness prognoses have been obtained routinely by the first (Eulerian) method for a period of about five months. In broad aspect the forecasts have represented reasonably good fits to the corresponding 500 mb forecasts.

However, they have suffered from certain characteristic deficiencies which have detracted from their usefulness. By 36 hours pressure patterns often tend to become ragged and distorted. In certain cases extreme exaggerations develop in which highs assume the appearance of intense lows, ridges elongate unnaturally and acquire a teardrop shape, and sharp troughs thrust southeastward from low centers.

Only limited testing has been possible with the Lagrangian Solution.

However, comparison of six cases tested to date with the corresponding Eulerian Solutions lends strong support to the following conclusions:

- (1) The Lagrangian forecasts are smoother and more realistic appearing.
- (2) The characteristic types of extreme exaggeration noted above are generally either eliminated or improved by the Lagrangian Solutions.
- (3) Overdevelopment of highs and, to a lesser extent, lows is a feature of both solutions, and apparently is a defect of the two-level model.

ACKNOWLEDGEMENTS

The author would like to express his sincere appreciation to Dr. Frederick G. Shuman for valuable help and counsel, to Mr. Harlan K. Saylor for his constant encouragement and his assistance in evaluation of results, and to Mrs. Joy McClees, Mrs. Lena Loman and Mr. James E. McDonell for their assistance in programming.

REFERENCES

- Estoque, M. A., 1957: Graphical integration of a two-level model. J. Meteor., 14, 38-42.
- Fjortoft, R., 1952: On a numerical method of integrating the barotropic vorticity equation. Tellus, 4, 179-194.
- Gates, W. L., 1959: On the truncation error, stability and convergence of difference solutions to the barotropic vorticity equation. J. Meteor., 16, 556-568.
- Knox, J. B., 1961: Numerical errors in time integration of advective processes. J. Geophys. Res., 66, 4177-4186.
- Obukhov, A. M., 1957: The accuracy of computation of advective variations of fields in quantitative forecasting of weather. Bull. Acad. Sci. USSR, Geophys. Serv., 63-72 (AGU translation).
- Okland, H., 1962: An experiment in numerical integration of the barotropic equation by a quasi-Lagrangian method. Geophys-Publ. 10 pp.
- Phillips, N. A., 1959: An example of non-linear computational instability, The Rossby Memorial Volume, Rockefeller Institute Press, New York.
- Phillips, N. A., 1960: Numerical Weather prediction, in Advances in Computers Vol. I., Academic Press, New York, 43-90.
- Reed, R. J., 1957: A graphical method for preparing 1000 millibar prognostic charts. J. Meteor., 14, 65-70.
- Reed, R. J., 1958: A graphical prediction model incorporating a form of nonadiabatic heating. J. Meteor., 15, 1-8.
- Reed, R. J., 1960: On the practical use of graphical prediction methods. Mon. Wea. Rev., 88, 209-218.
- Shuman, F. G., 1957: Predictive consequences of certain physical inconsistencies in the geostrophic barotropic model. Mon. Wea. Rev., 85, 229-234.

APPENDIX

1. Accuracy of the trajectory method

By definition

$$u = dx/dt, \quad v = dy/dt$$

Thus the displacements in the x and y directions during a finite interval

of time are

$$\delta x = \int u(x, y, t) dt$$

$$\delta y = \int v(x, y, t) dt$$

Expanding now the integrand in a Taylor Series about x_0, y_0, t_0 and omitting

higher order terms, we find that

$$\delta x = \int \left[u_0 + \left(\frac{\partial u}{\partial x} \right)_0 \delta x + \left(\frac{\partial u}{\partial y} \right)_0 \delta y + \left(\frac{\partial u}{\partial t} \right)_0 \delta t + \dots \right] dt$$

$$\delta y = \int \left[v_0 + \left(\frac{\partial v}{\partial x} \right)_0 \delta x + \left(\frac{\partial v}{\partial y} \right)_0 \delta y + \left(\frac{\partial v}{\partial t} \right)_0 \delta t + \dots \right] dt$$

or

$$\delta x = \int_0^t \left[u_0 + \left(u \frac{\partial u}{\partial x} \right)_0 \delta t + \left(v \frac{\partial u}{\partial y} \right)_0 \delta t + \left(\frac{\partial u}{\partial t} \right)_0 \delta t + \dots \right] dt$$

$$\delta y = \int_0^t \left[v_0 + \left(u \frac{\partial v}{\partial x} \right)_0 \delta t + \left(v \frac{\partial v}{\partial y} \right)_0 \delta t + \left(\frac{\partial v}{\partial t} \right)_0 \delta t + \dots \right] dt$$

Thus

$$\delta x = u_0 t + \left(\frac{\partial u}{\partial t} + u \frac{\partial u}{\partial x} + v \frac{\partial u}{\partial y} \right)_0 \frac{t^2}{2} + \dots$$

$$\delta y = v_0 t + \left(\frac{\partial v}{\partial t} + u \frac{\partial v}{\partial x} + v \frac{\partial v}{\partial y} \right)_0 \frac{t^2}{2} + \dots$$

The terms in parenthesis will be recognized as the component accelerations at the origin. These will be roughly an order of magnitude smaller than the coriolis acceleration. Hence, the ratio of the second term to the first is

$$r = \frac{fu_0}{10} \frac{t^2}{2} / u_0 t = \frac{ft}{20}$$

For $f = 10^{-4} \text{ sec}^{-1}$, $t = 3600 \text{ sec}$ (one hour)

$$r = 0.018$$

It is apparent that for the short time interval employed here, the displacement error in using only the first term in the series is very small.

2. The bi-linear interpolation formula

Let i, j be the grid indices increasing in the manner shown in figure 13, and α be

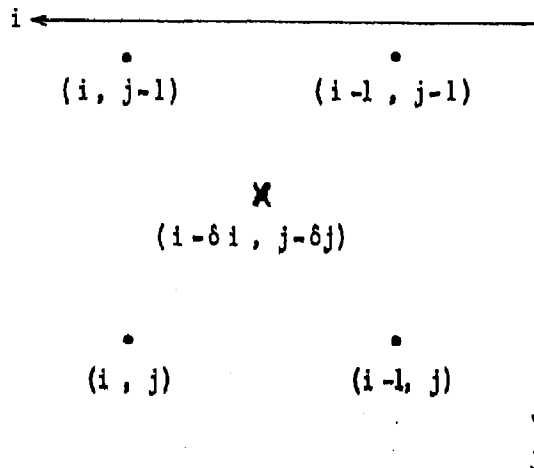


Figure 13

Grid scheme used in bi-linear interpolation

the wind displacement. Successive linear interpolations in the i and j directions gives for α at an interior point $(i-\delta i, j-\delta j)$

$$\alpha_{i-\delta i, j-\delta j} = \alpha_{i,j} + (\alpha_{i-1,j} - \alpha_{i,j}) \delta i + (\alpha_{i,j-1} - \alpha_{i,j}) \delta j + (\alpha_{i,j} + \alpha_{i-1,j-1} - \alpha_{i,j-1} - \alpha_{i-1,j}) \delta i \delta j$$

3. The bi-quadratic interpolation formula

Consider an array of 16 points, as shown in figure 14, surrounding an interior point p at which it is desired to make the interpolation. The interpolated value of

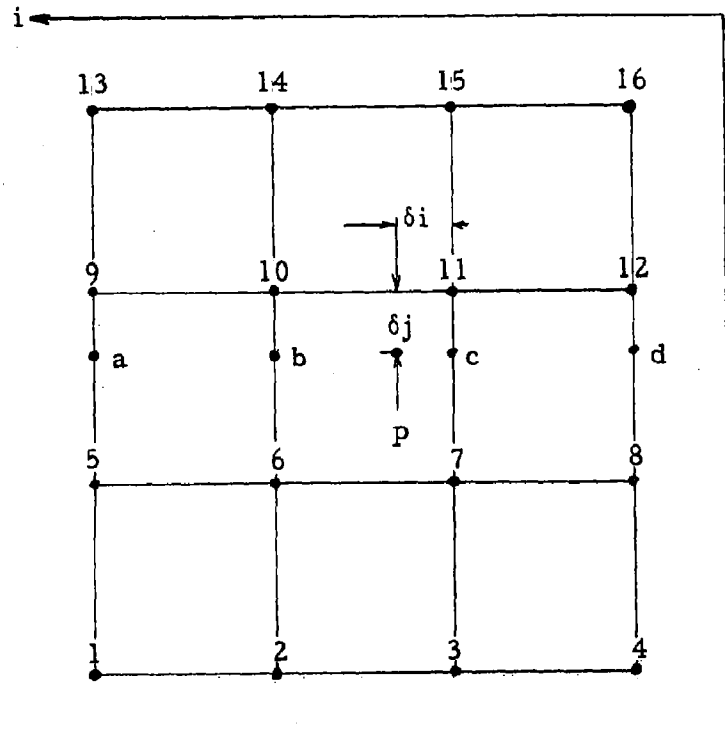


Figure 14

Grid scheme used in bi-quadratic interpolation

a variable β at point a, derived from a quadratic curve which passes through points 5 and 9 and is the least square fit to points 1 and 13, is

$$\beta_a = \frac{1}{4} [(\delta j)^2 - \delta j](\beta_1 - \beta_5 - \beta_9 + \beta_{13}) + \delta j(\beta_5 - \beta_9) + \beta_9$$

Similar formulas apply at points b, c, and d. A quadratic interpolation in the i direction then gives

$$\beta_p = \frac{1}{4} [(\delta i)^2 - \delta i](\beta_a - \beta_b - \beta_c + \beta_d) + \delta i(\beta_b - \beta_c) + \beta_c$$

4. The 16-point averaging formula

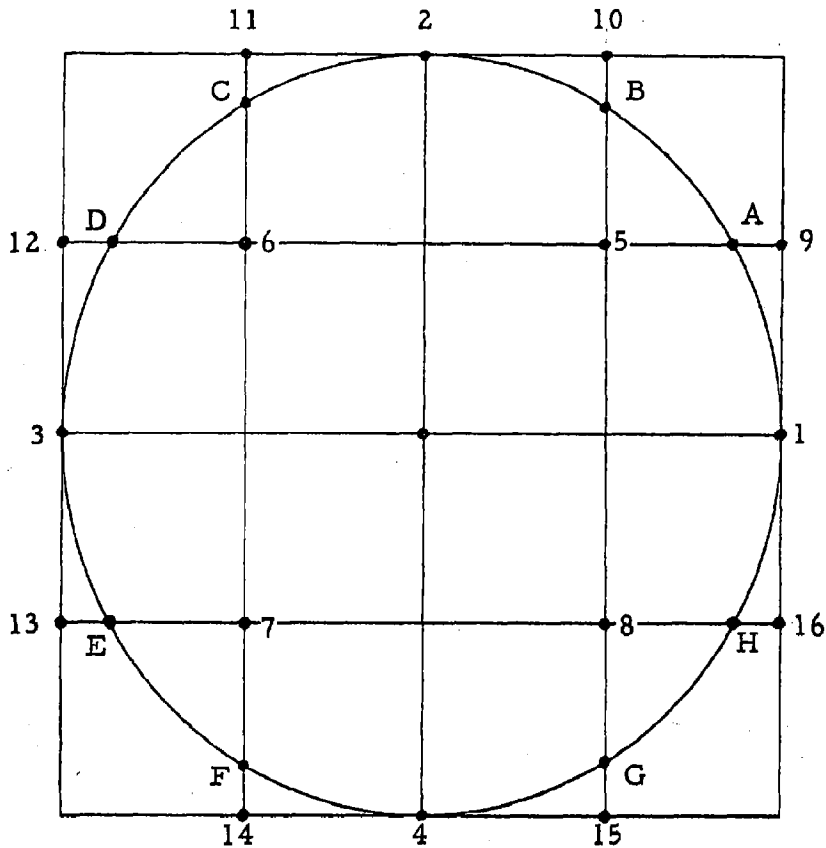


Figure 15

Grid scheme used in 16-point averaging

The average value of a variable \bar{z} around the circle with radius twice the mesh length (figure 15) is

$$\bar{z} = (z_1 + z_2 + z_3 + z_4 + z_A + z_B + z_C + z_D + z_E + z_F + z_G + z_H) / 12$$

From the geometry

$$z_A = z_5 + 0.732(z_9 - z_5)$$

and similar equations apply to z_B etc.

Thus

$$\begin{aligned} \bar{z} = & 0.0833(z_1 + z_2 + z_3 + z_4) + 0.0446(z_5 + z_6 + z_7 + z_8) \\ & + 0.061(z_9 + z_{10} + z_{11} + z_{12} + z_{13} + z_{14} + z_{15} + z_{16}) \end{aligned}$$

LEGENDS

- Fig. 1. 36-hr 1000 mb prognosis verifying at 12Z, March 22, 1962. Example of accurate Eulerian forecast. (Compare with figure 2)
- Fig. 2. Surface map 12Z, March 22, 1962.
- Fig. 3. 36-hr 1000 mb prognosis verifying at 00Z, April 15, 1962. Example of poor Eulerian forecast, especially in region south of Newfoundland.
- Fig. 4. Surface map, 00Z, February 28, 1962. Dashed lines indicate estimated streamlines in absence of friction.
- Fig. 5. 850 mb map, 00Z February 28, 1962. Note that winds and isotherms between Amarillo and Big Spring suggest that the true surface gradient is more in conformity with the streamlines in fig. 4 than with the reduced isobars. Note, too, that the contours and isotherms in this figure should be discontinuous over the Rockies.
- Fig. 6. Illustration of boundary (dashed line) separating interior and exterior regions.
- Fig. 7. 36-hr 1000 mb prognosis verifying at 00Z, April 15, 1962, Lagrangian Solution.
- Fig. 8. Surface map 00Z, April 15, 1962.
- Fig. 9. 500 mb initial contour chart and conservative quantity (dashed), 12Z, April 13, 1962.
- Fig. 10. 12 hr forecast of 500 mb contours and conservative quantity (dashed), verifying 12Z, April 14, 1962.
- Fig. 11. 24 hr forecast of 500 mb contours and conservative quantity (dashed),

verifying 12Z, April 14, 1962.

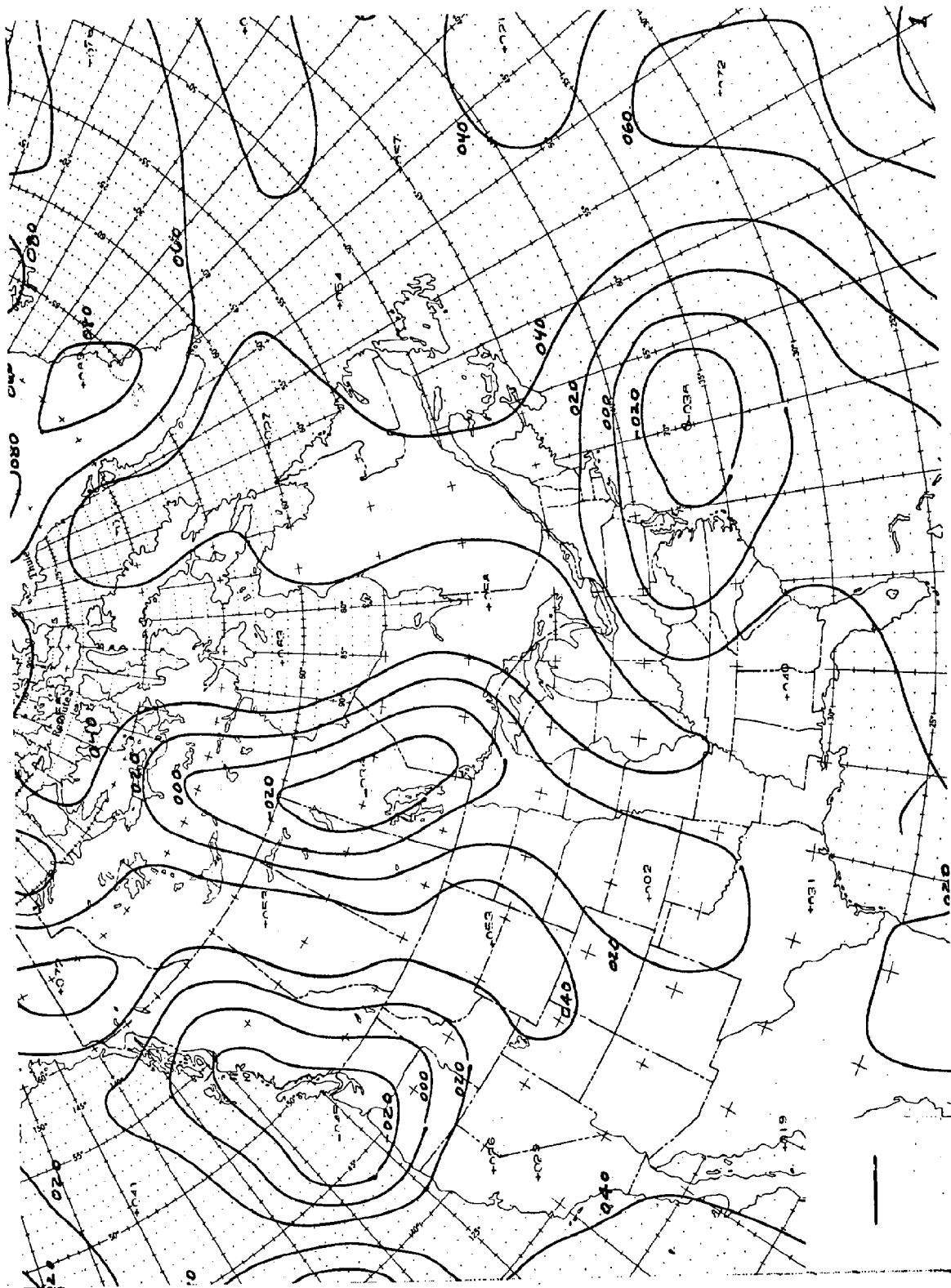
Fig. 12. 36 hr forecast of 500 mb contours and conservative quantity (dashed),

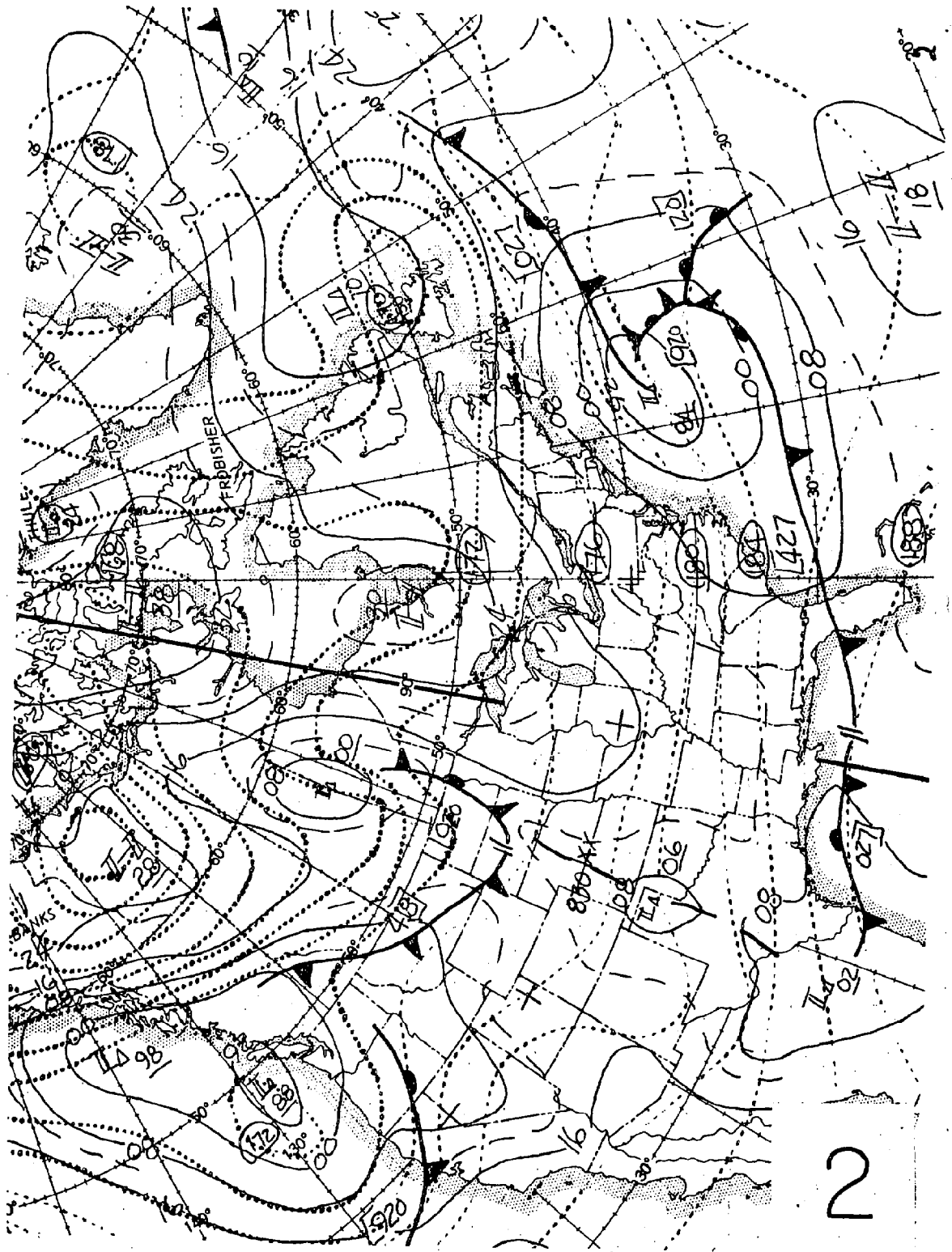
verifying 00Z, April 15, 1962.

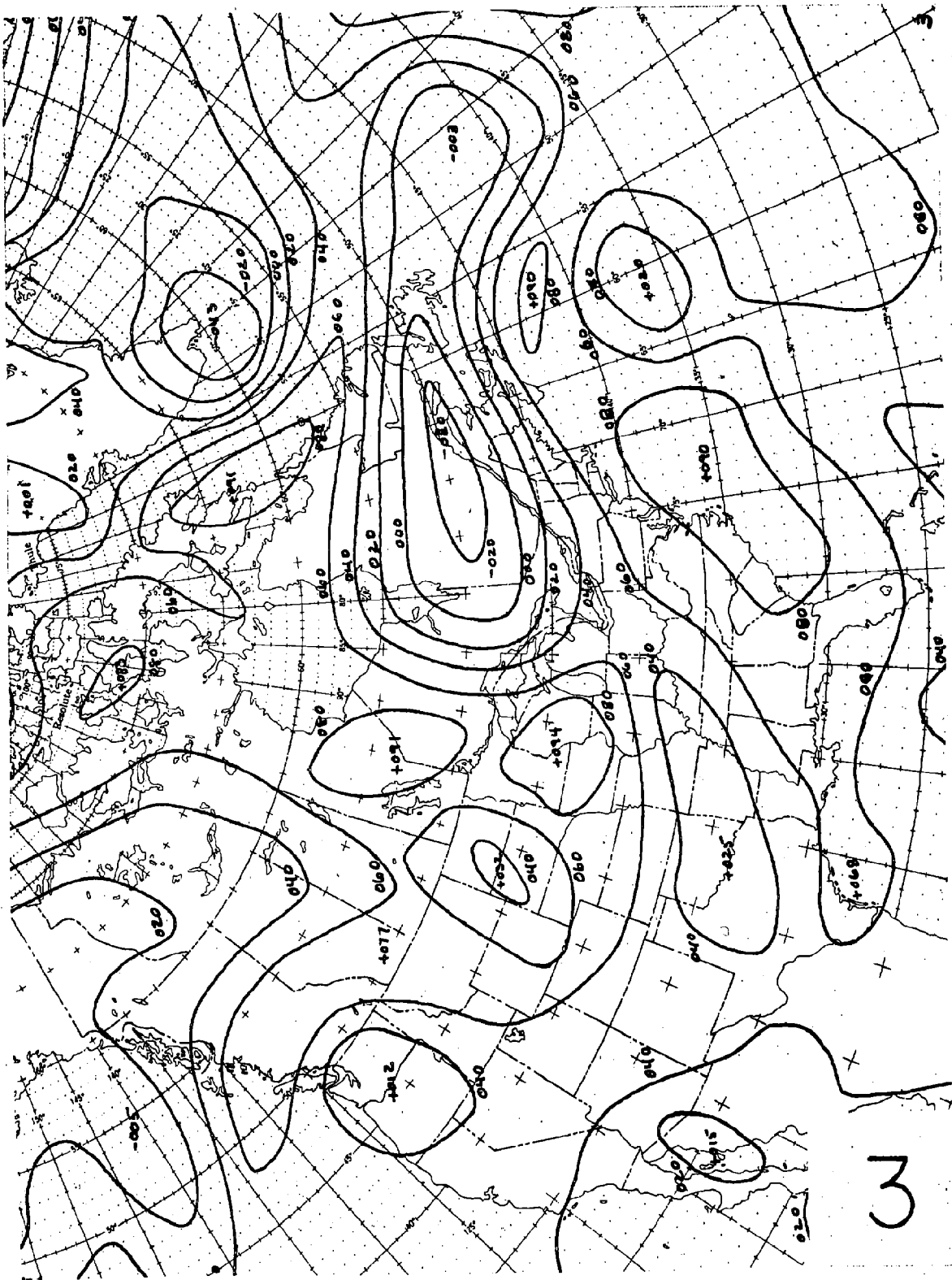
Fig. 13. Grid scheme used in bi-linear interpolation.

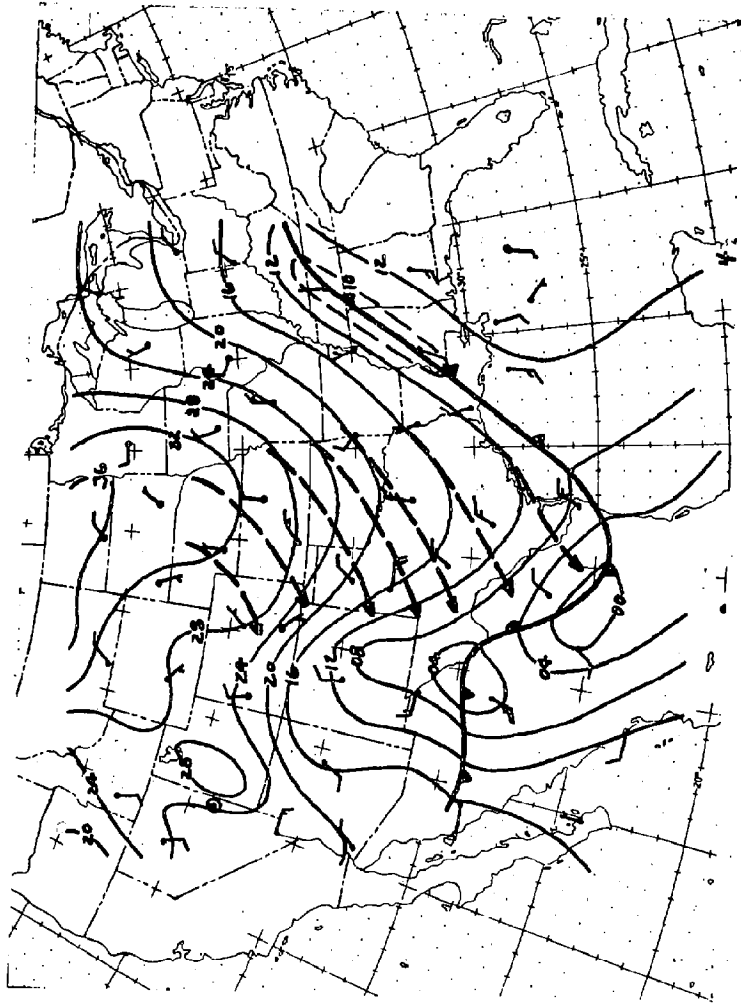
Fig. 14. Grid scheme used in bi-quadratic interpolation.

Fig. 15. Grid scheme used in 16-point averaging.

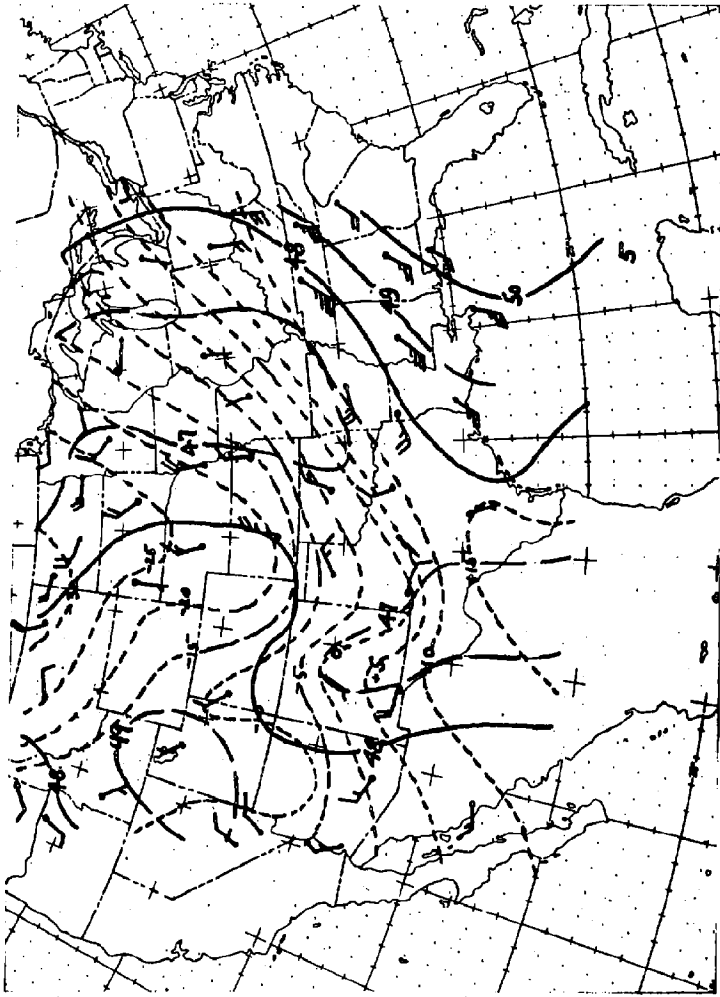


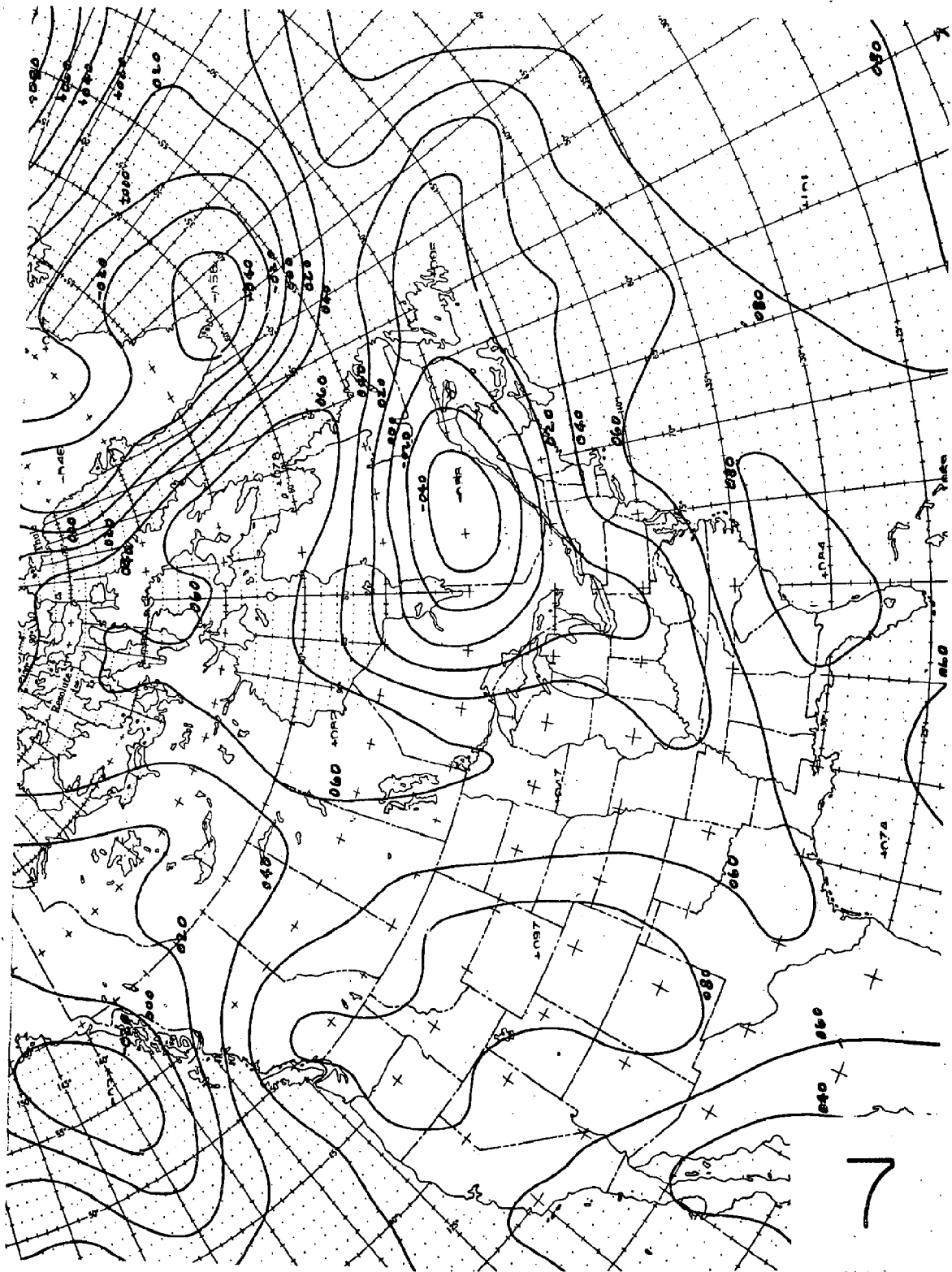


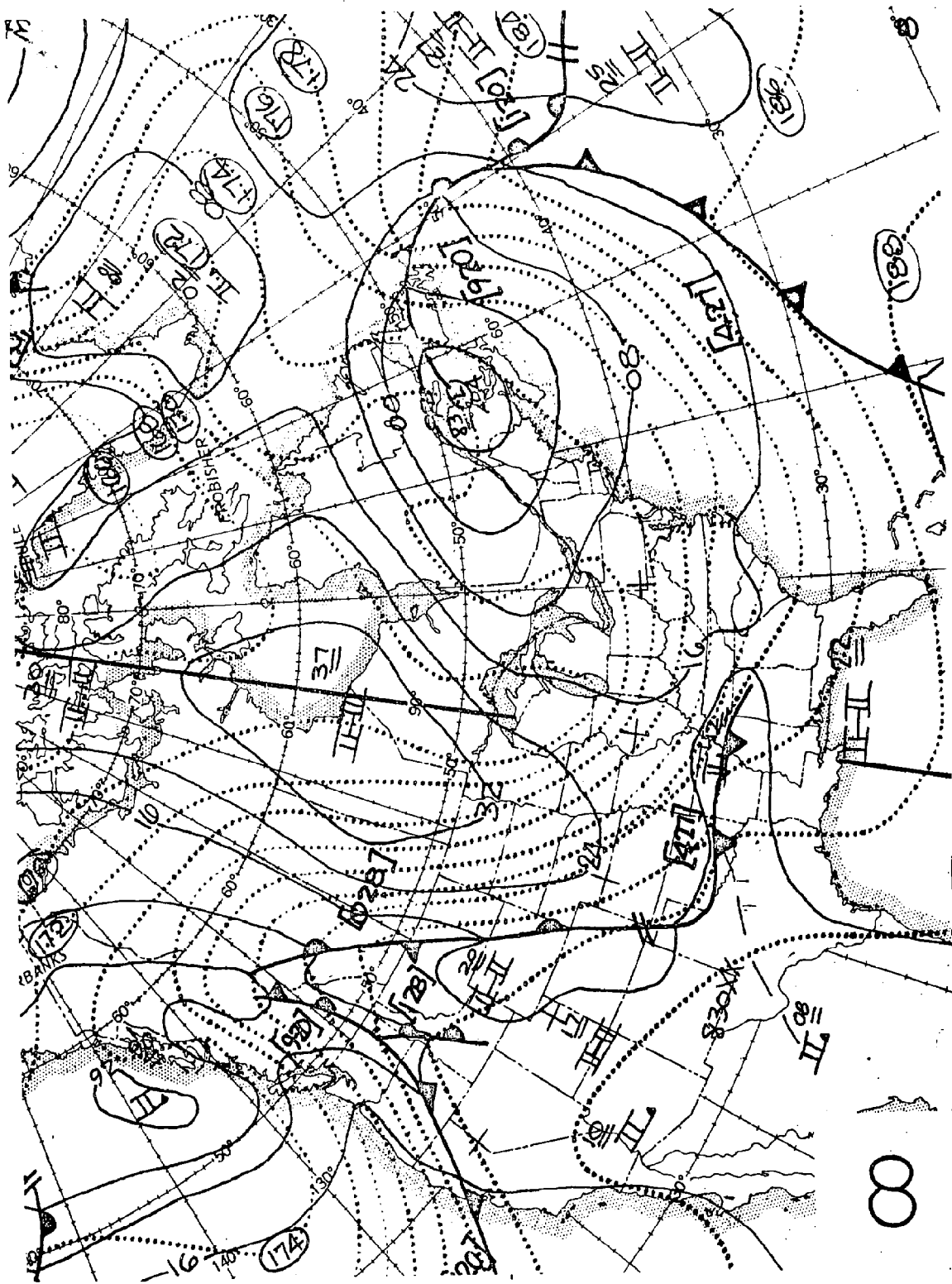


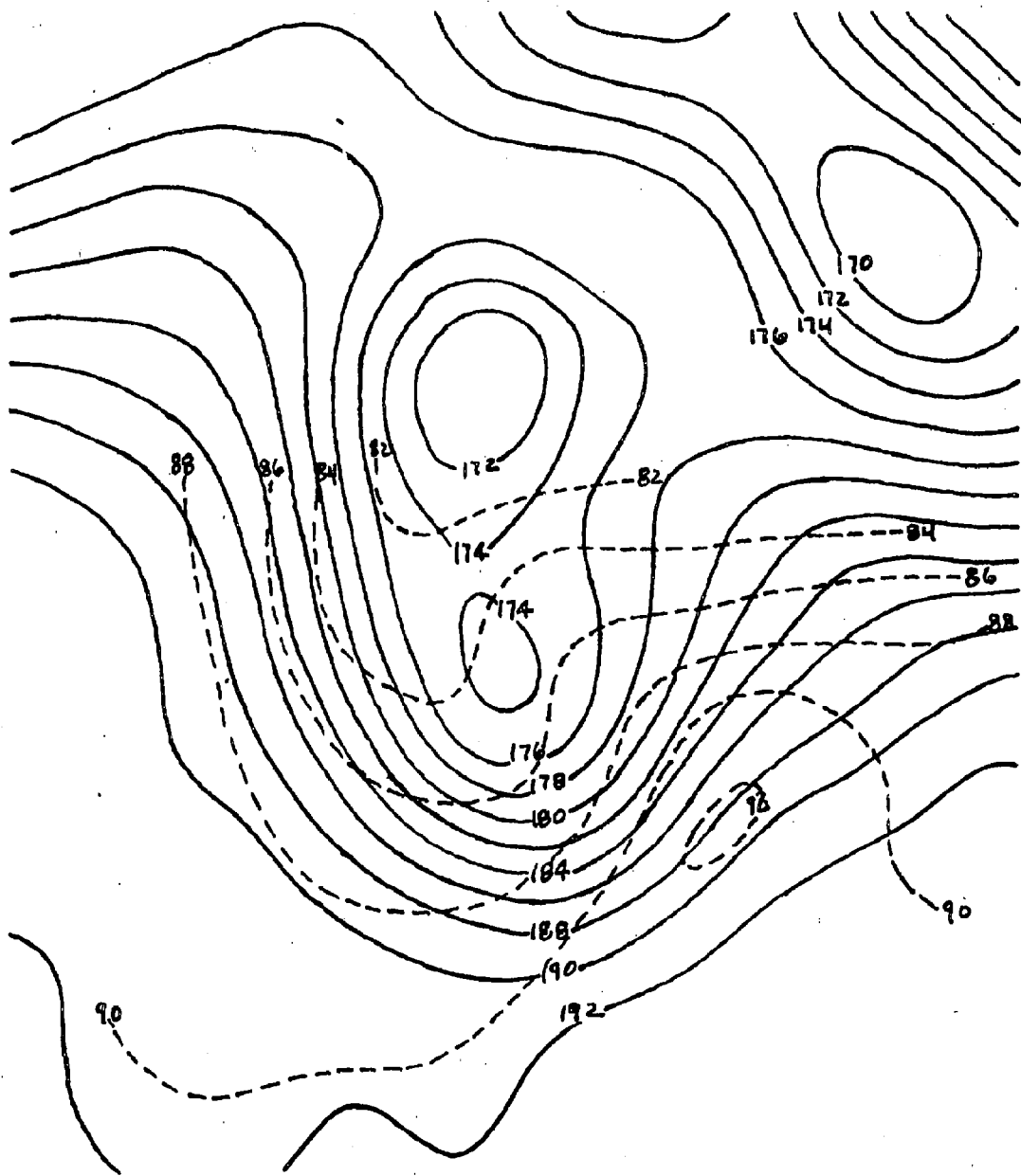


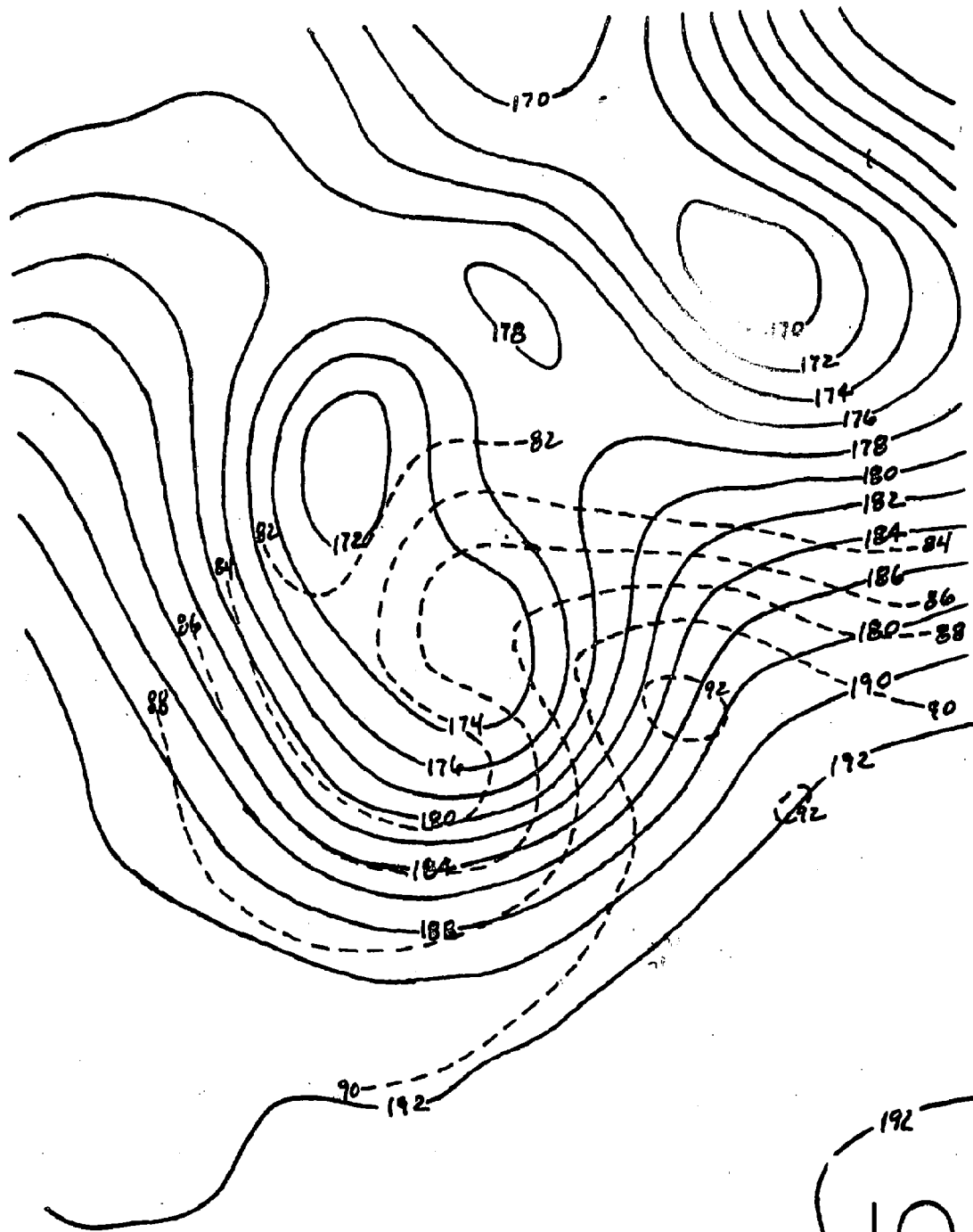
4











10

